Supporting Information
Abundance of liquid, internally mixed particles in the North Atlantic free troposphere during summertime

Zezhen Cheng[1], Megan Morgenstern[2], Bo Zhang[3], Matthew Fraund[4], Nurun Nahar Lata[1], Rhenton Brimberry[1], Matthew A. Marcus[4], Lynn Mazzoleni[2], Paulo Fialho[5], Silvia Henning[6], Birgit Wehner[6], Claudio Mazzoleni[2], Swarup China[1]

[1] Environmental Molecular Sciences Laboratory, Pacific Northwest National Laboratory (PNNL), Richland, Washington 99352, USA

[2] Atmospheric Sciences Program, Michigan Technological University, Houghton, Michigan, 49921, USA

[3] National Institute of Aerospace, Hampton, VA 23666, USA

[4] Advanced Light Source, Lawrence Berkeley National Laboratory, Berkeley, CA 94720, USA

[5] Institute of Volcanology and Risk Assessment – IVAR, Rua da Mãe de Deus, 9500-321 Ponta Delgada, Portugal

[6] Leibniz Institute for Tropospheric Research, Permoserstraße 15, 04318 Leipzig, Germany

Correspondence to: Swarup China (Swarup.china@pnnl.gov)

Glass transition temperature prediction

A range of glass transition temperature ($T_{g,org}$) for organic aerosols from June to July 2017 as a function of relative humidity (RH) has been estimated following the methods introduced by (Wang et al. 2012):

$$T_{g,org}(RH) = \frac{T_{g,w}k_{GT} + f(RH)T_{g,org}(RH=0\%)}{k_{GT} + f(RH)}, \quad (S1)$$

where

$$f(RH) = \frac{100-RH}{RH}\frac{1}{\kappa_{org}}\frac{\rho_{org}}{\rho_w}, \quad (S2)$$

where $T_{g,w}$ is equal to 136 K, is the T_g for pure water, k_{GT} is the Gordon-Taylor constant, κ_{org} is the CCN-derived hygroscopicity parameter of the organic fraction, ρ_{org} and ρ_w are the density of water and organic material, respectively. In this study, we cannot retrieve T_g(RH = 0%) for particles. Therefore, we adopted previously reported values for these parameters, which were also retrieved at the Pico Mountain Observatory but on 27–28 June 2013, 5–6 July 2014, and 20–21 June 2015 (Schum et al. 2018). However, the T_g(RH = 0%) of these sampling periods is very stable (Schum et al. 2018). Therefore, we used the average value of T_g(RH = 0%) reported by (Schum et al. 2018) (332.09 K) to predict T_g of particles in this study, and the highest and lowest value of T_g(RH = 0%) reported by (Schum et al. 2018) (360.65K and 313.46K, respectively) as upper and lower bound. Moreover, k_{GT}, $T_{g,w}$, κ_{org}, and ρ_{org} were assumed to be 2.5

(Shiraiwa et al. 2017), 309 K (Schum et al. 2018), 0.12 (Schum et al. 2018), and 1.4 g cm^{-3} (Schum et al. 2018), respectively.

CCSEM-EDX Atomic Percentage Correction

EDX analysis of light elements such as C, N, and O is considered semi-quantitative, and C and O contributions from the B-film substrate. Therefore, we performed post-correction on the elemental percentage of C, N, and O. To do this, we used CNQX disodium salt (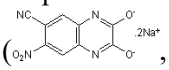 , CAS Number: 479347-85-8) as standard material, which has advantages such as 1) containing C, N, and O; 2) contain Na, which EDX can quantitatively analyze; 3) CNQX disodium salt is stable under the electrical beam; 4) CNQX disodium salt is soluble in the water so that we can generate CNQX disodium salt particles by nebulizing 0.5 g L^{-1} solution; 5) shape of CNQX disodium salt particle is spheric (see Fig. S1). Therefore, we performed CCSEM-EDX analysis on CNQX disodium salt particles and retrieved the following correction function for C, N, and O:

$$\mathrm{C_{real}} = (123.2 \pm 1.4) - (4.738 \pm 0.214)\log(\mathrm{H}) - (1.186 \pm 0.02)\mathrm{C_{measured}}, \mathrm{R^2} = 0.8484, \quad \text{(S3)}$$

$$\mathrm{O_{real}} = (13.68 \pm 0.18) - (0.3413 \pm 0.0636)\log(\mathrm{H}) + (0.2579 \pm 0.0072)\mathrm{O_{measured}}, \mathrm{R^2} = 0.937, \quad \text{(S4)}$$

$$\mathrm{N_{real}} = (1.101 \pm 0.002)\mathrm{N_{measured}}, \mathrm{R^2} = 0.791, \quad \text{(S5)}$$

Where $C_{measured}$, $N_{measured}$, and $O_{measured}$ are measured atomic percentages of C, N, and O, respectively, C_{real}, N_{real}, and O_{real} are expected atomic percentages of C, N, and O, respectively, which are calculated based on the stoichiometric ratio between that element and Na, and H is the hight of the particle (μm). Since the particles are spheric, the measured area equivalent diameter (μm) is approximately equal to the height of particles. Therefore, when applying the correction function on our CCSEM-EDX data, we need to estimate the H by dividing the longest diameter retrieved from CCSEM-EDX measurement by the aspect ratio retrieved from tilted images (see Sect. 3.3.2).

Table S1. Additional information of Pico 2014 and Pico 2015 samples.

Sample ID	SA1	SA2	SA3	S1	S2	S3	S4	S5	S6
Date	4 July 2014	10 July 2014	12 July 2014	20 June 2015	26 June 2015	3 July 2015	10 July 2015	19 July 2015	26 July 2015
Time started	15:49	17:24	15:07	15:15	15:22	15:20	17:10	13:38	8:30
Time ended	21:00	20:22	18:33	15:50	17:58	19:09	18:40	17:51	15:00
# of STXM-NEXAFS analyzed particle	653	208	425	NA	NA	86	NA	37	NA
OC	5.4%	7.7%	8.7%	NA	NA	68.6%	NA	21.6%	NA
OCIN	82.7%	20.4%	76.9%	NA	NA	3.5%	NA	35.1%	NA
OCEC	2.0%	2.5%	0.5%	NA	NA	24.4%	NA	5.4%	NA
OCECIN	10.0%	6.6%	13.9%	NA	NA	3.5%	NA	37.8%	NA

Table S2. Additional information of Pico 2017 samples. S3 and S4 mean samples were collected at stage 3 (cut-off size: >0.15 μm) and stage 4 (cut-off size: >0.05 μm) of an MPS-4G1impactor, respectively.

Sample ID	S3-1	S3-2	S3-3	S3-4	S4-1	S4-2	S4-3	S4-4
Date	24 June 2017	27 June 2017	27 June 2017	29 June 2017	6 July 2017	9 July 2017	27 July 2017	29 July 2017
Time started	15:23	14:00	16:45	14:30	13:40	12:51	14:04	11:39
Time ended	17:23	14:22	17:15	15:00	14:20	14:01	14:14	11:51
# of CCSEM-EDX Analyzed Particles	726	968	2573	1943	753	984	1503	592
OC (%)	6.3	6.7	14.1	4.2	16.6	13.5	2.4	9.8
CNO (%)	23.4	62.2	39.6	55.2	27.0	35.2	43.7	32.1
CNOS (%)	0.1	0.1	0.0	0.0	0.1	0.1	0.7	0.5
Sea salt (%)	28.2	8.9	28.0	11.3	19.4	28.9	24.8	31.6
sea salt/S (%)	31.5	17.6	14.1	27.4	5.2	13.3	22.8	13.5
Dust (%)	1.1	1.1	0.7	0.6	0.3	0.1	0.2	0.3
Sulfate coated dust (%)	0.1	0.1	0.1	0.0	0.1	0.0	0.2	0.2
Others (%)	9.1	3.3	3.5	1.4	31.3	8.9	5.2	12.0
# of STXM-NEXAFS analyzed particle	NA	NA	140	NA	166	NA	NA	NA
OC (%)	NA	NA	6.4	NA	1.2	NA	NA	NA
OCIN (%)	NA	NA	86.4	NA	98.8	NA	NA	NA
OCEC (%)	NA	NA	0.0	NA	0.0	NA	NA	NA
OCECIN (%)	NA	NA	7.1	NA	0.0	NA	NA	NA
Temperature measured at OMP (K)	NA	NA	285.0	286.6	287.8	284.9	287.5	285.9
Temperature from FLEXPART (K)	280.8	285.9	286.1	283.7	284.4	282.3	288.0	284.3
RH at OMP (%)	NA	NA	26.8	49.7	31.3	6.7	11.5	22.0
RH from FLEXPART (%)	23.2	33.1	31.4	37.3	27.5	10.2	17.98	15.2
$T_{g,org}$ at site from meteorological data (K)	NA	NA	315.7	293.3	312.0	328.6	325.9	319.2
$T_{g,org}$ at site from FLEXPART data (K)	318.3	310.5	311.9	306.7	315.1	326.7	321.9	323.7

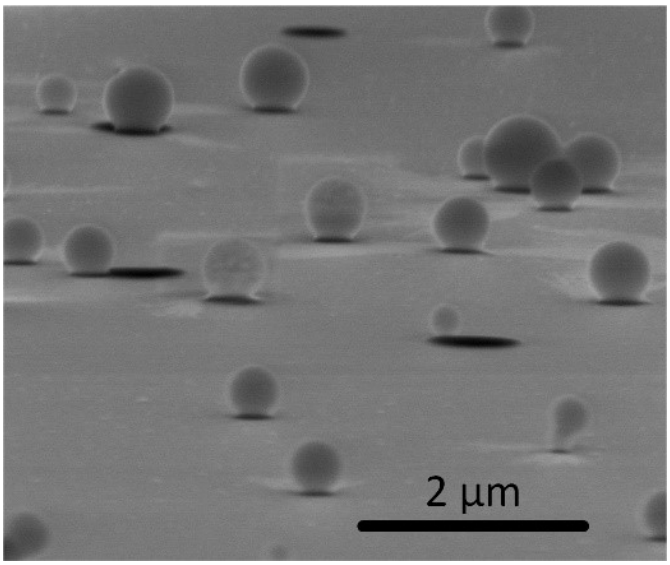

Figure S1. Representative tilted image of CNQX disodium salt particle generated from nebulizing 0.5 g L^{-1} aquatic solution.

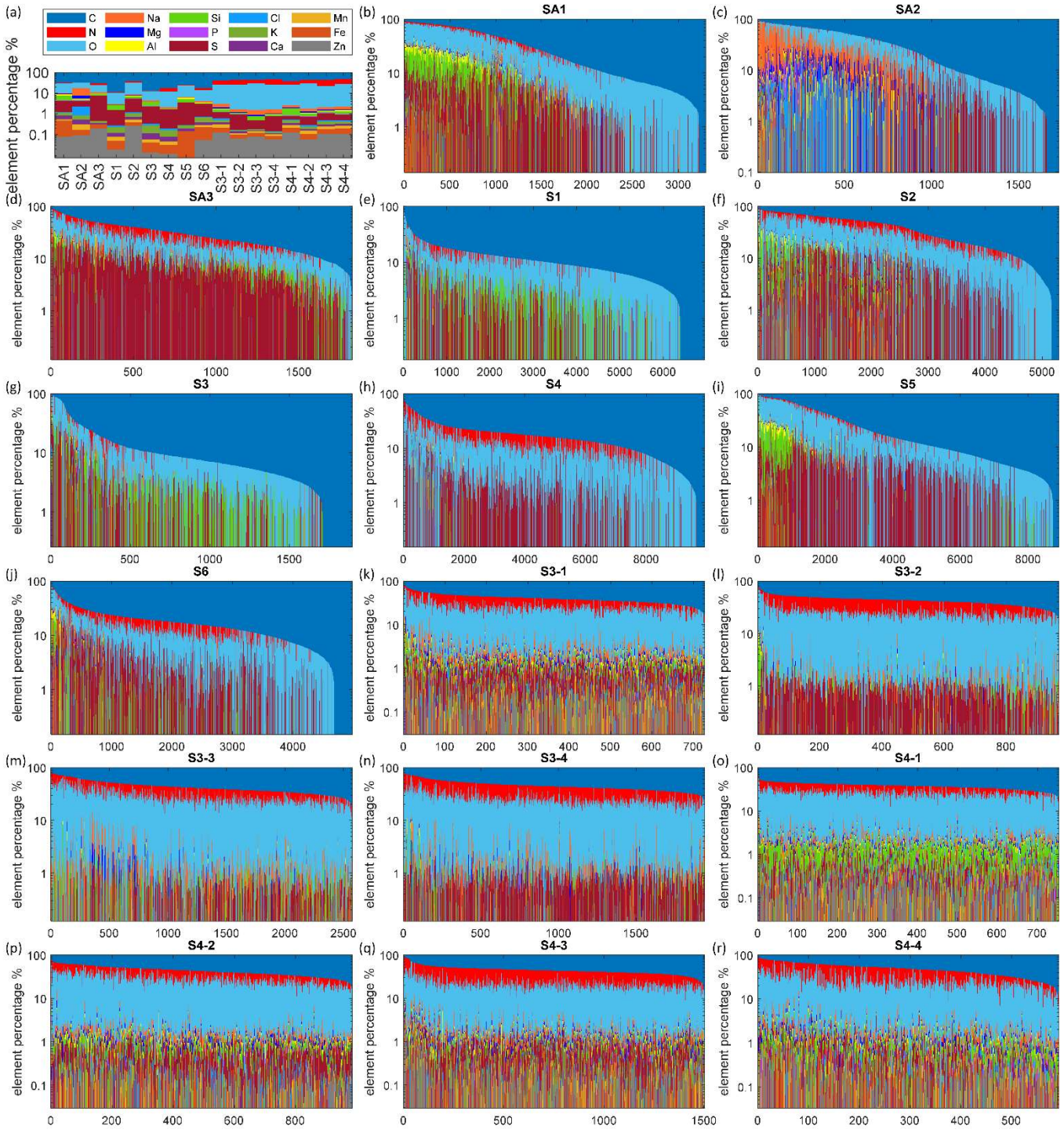

Figure S2. Relative atomic ratios of 15 elements (C, N, O, Na, Mg, Al, Si, P, S, Cl, K, Ca, Mn, Fe, Zn) for (a) average relative atomic ratios for all samples, (b) SA1, (c) SA2, (d) SA3, (e) S1, (f) S2, (g) S3, (h) S4, (i) S5, (j) S6, (k) S3-1, (l) S3-2, (m) S3-3, (n) S3-4, (o) S4-1, (p) S4-2, (q) S4-3, (r) S4-4.

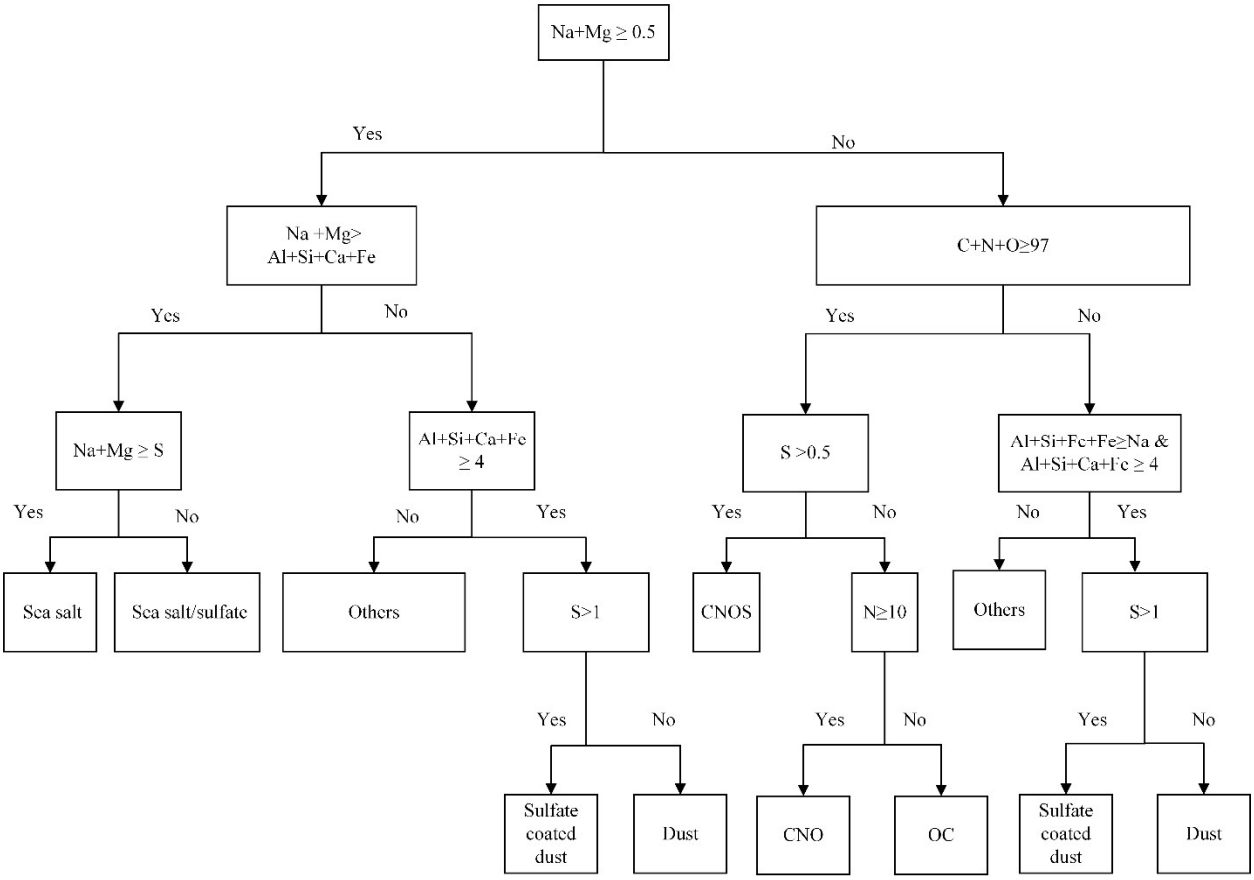

Figure S3. Flow chart to classify Pico 2017 particle types based on their relative element weight percent retrieved from CCSEM/EDX measurements.

75

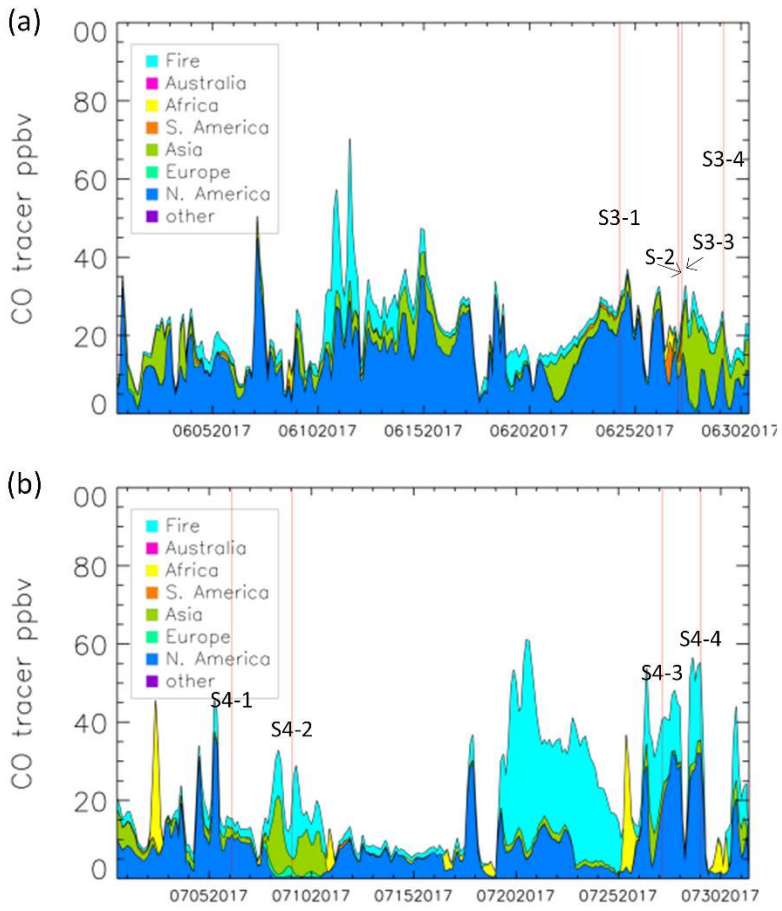

Figure S4. FLEXPART CO tracer simulation for (a) Jun 2017 and (b) July 2017.

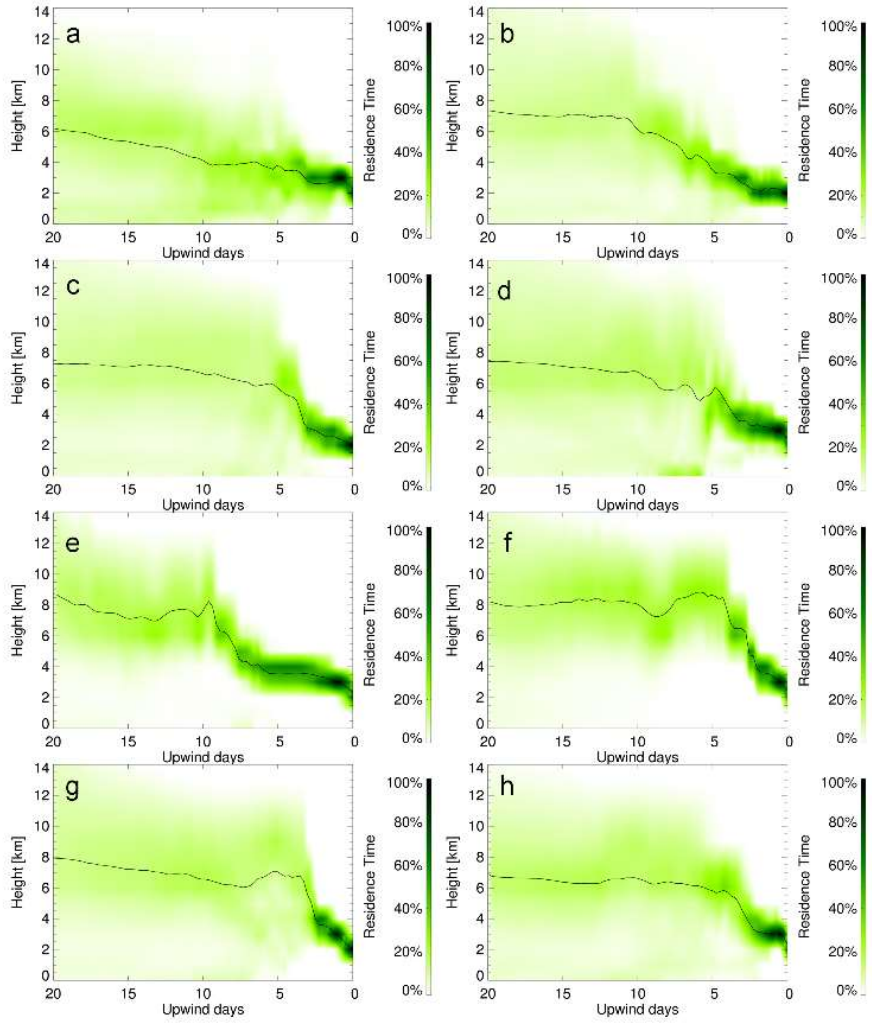

Figure S5. The vertical distribution of the retroplumes residence time at given upwind times retrieved from FLEXPART retroplumes for (a) S3-1, (b) S3-2, (c) S3-3, (d) S3-4, (e) S4-1, (f) S4-2, (g) S4-3, (h) S4-4, (i) S4-5.

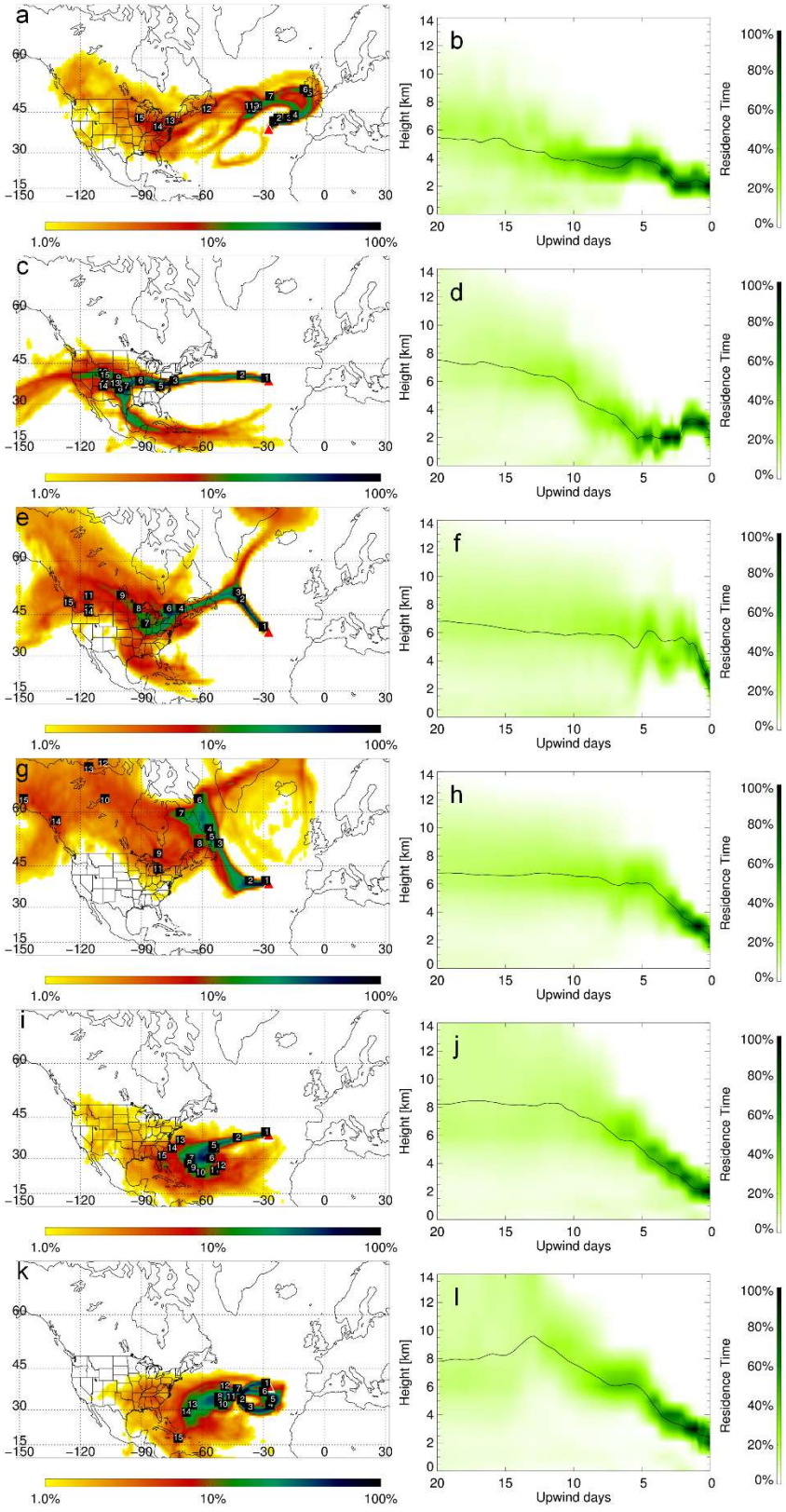
a
b
c
d
e
f
g
h
i
j
k
l
60
45
30
15
−150
−120
−90
−60
−30
0
30
1.0%
10%
100%
Height [km]
Upwind days
Residence Time
20%
40%
60%
80%

Figure S6. Column-integrated residence time over the 20-day transport time and the vertical distribution of the retroplumes residence time at given upwind times retrieved from FLEXPART retroplumes for Pico 2015. (a,b) S1, (c,d) S2, (e,f) S3, (g,h) S4, (i,j) S5, (k,l) S6.

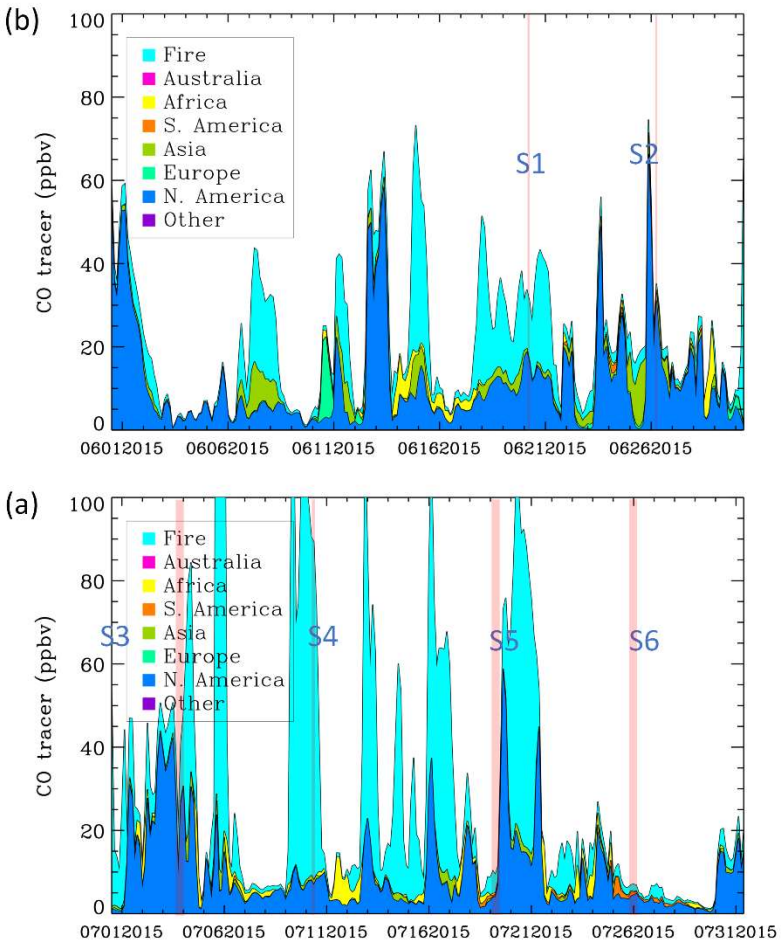

Figure S7. FLEXPART CO tracer simulation for (a) Jun 2015 and (b) July 2015.

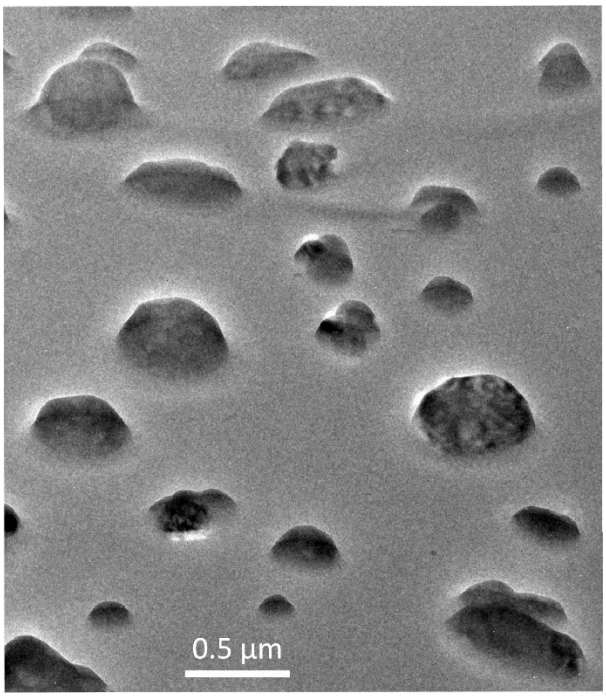

Figure S8. Representative tilted transmission electron microscopy (TEM, the titled angle was 70°) of S3-2.

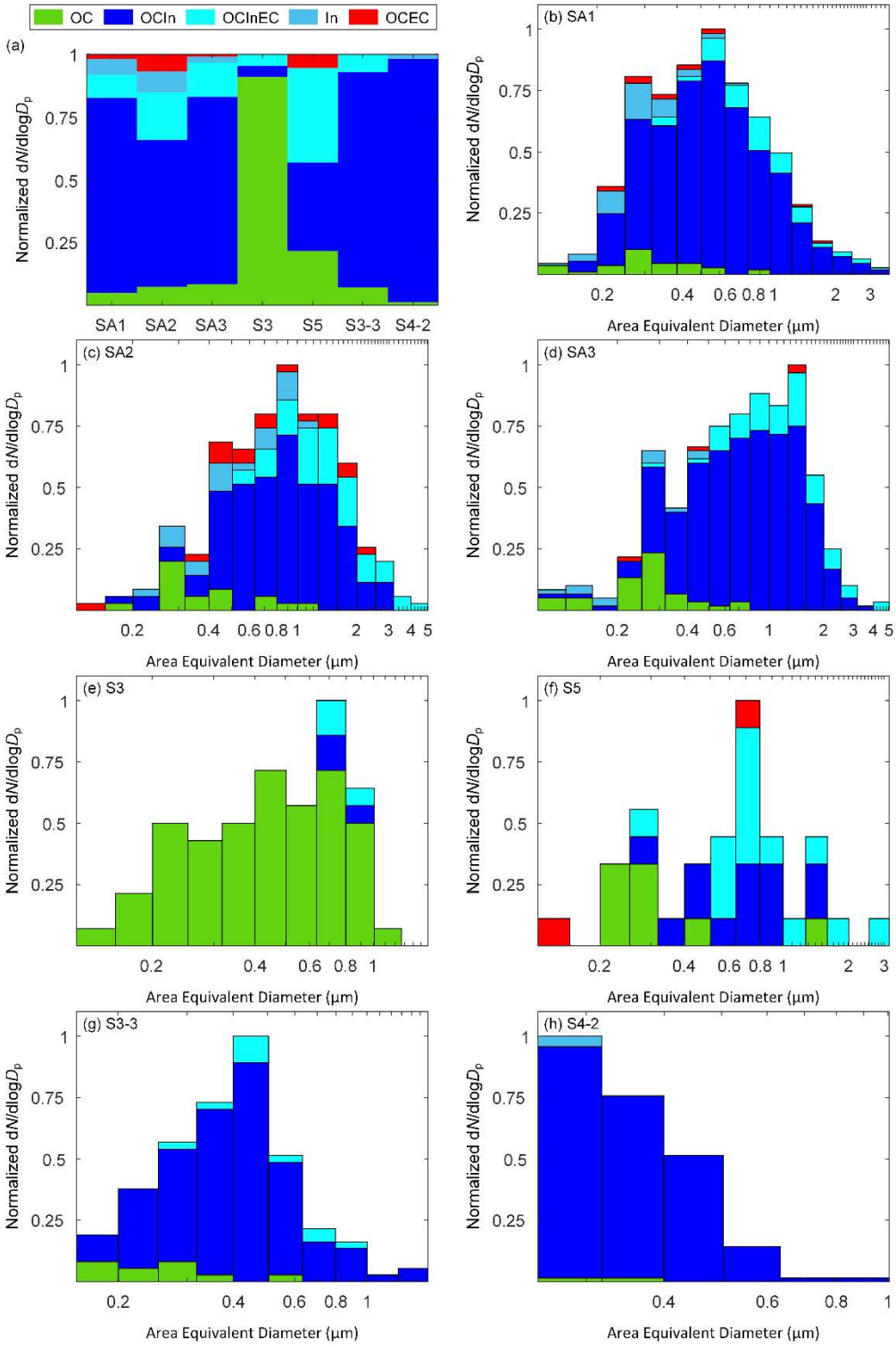

95

Figure S9. Chemically resolved size distributions inferred from the STXM-NEXAFS measurements for samples. (a) Fraction of different particle types for all samples, size distributions of fraction (b) SA1, (c) SA2, (d) SA3, (e) S3, (f) S5, (g) S3-3, and (h) S4-2.

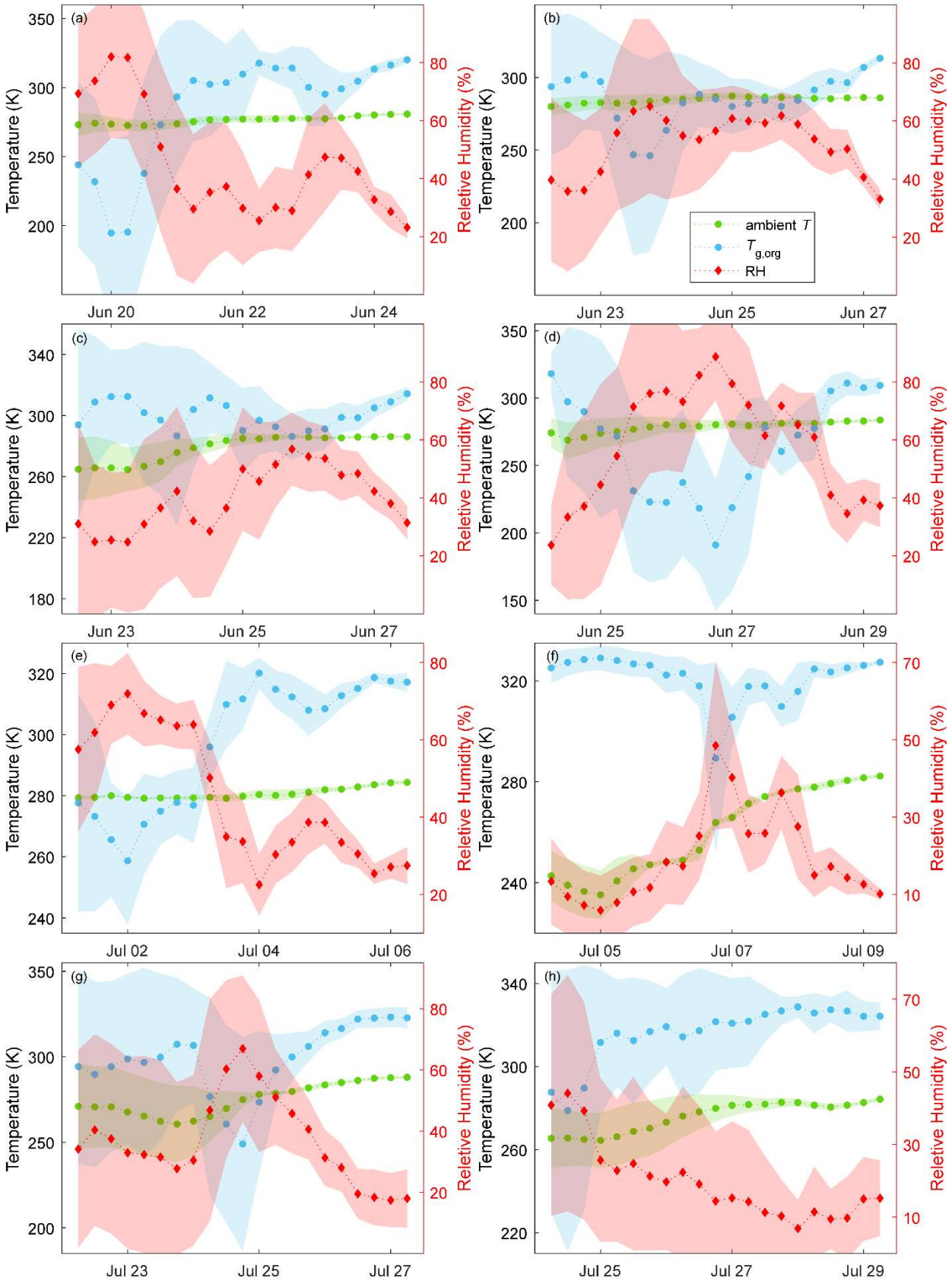
(a)
(b)
(c)
(d)
(e)
(f)
(g)
(h)
Temperature (K)
Reletive Humidity (%)
ambient T
$T_{g,org}$
RH
Jun 20
Jun 22
Jun 24
Jun 23
Jun 25
Jun 27
Jun 29
Jul 02
Jul 04
Jul 06
Jul 05
Jul 07
Jul 09
Jul 23
Jul 25
Jul 27
Jul 29

Figure S10. Mean ambient temperature (blue) and relative humidity (RH) (red) extracted from the GFS analysis along the FLEXPART modeled path weighted by the residence time and the predicted RH-dependent $T_{g,org}$ values (green) for (a) S3-1, (b) S3-2, (c) S3-3, (d) S3-4, (e) S4-1, (g) S3-2, (g) S4-3, (h) S4-4, and (i) S4-54. The blue and red shaded areas represent 1 standard deviation of ambient temperature and RH from the GFS analysis, respectively. The green shaded areas represent uncertainties of predicted $T_{g,org}$ estimated based on the range of $T_{g,org}$(RH = 0%) and uncertainties in RH (See SI).

References:

Ching, J., Adachi, K., Zaizen, Y., Igarashi, Y., and Kajino, M. (2019). Aerosol mixing state revealed by transmission electron microscopy pertaining to cloud formation and human airway deposition. *npj Clim. Atmos. Sci.* 2 (1):1–7. doi:10.1038/s41612-019-0081-9.

Froyd, K.D., Murphy, D.M., Brock, C.A., Campuzano-Jost, P., Dibb, J.E., Jimenez, J.L., Kupc, A., Middlebrook, A.M., Schill, G.P., Thornhill, K.L., Williamson, C.J., Wilson, J.C., and Ziemba, L.D. (2019). A new method to quantify mineral dust and other aerosol species from aircraft platforms using single-particle mass spectrometry. *Atmos. Meas. Tech.* 12 (11):6209–6239. doi:10.5194/amt-12-6209-2019.

Schum, S.K., Zhang, B., Dzepina, K., Fialho, P., Mazzoleni, C., and Mazzoleni, L.R. (2018). Molecular and physical characteristics of aerosol at a remote free troposphere site: Implications for atmospheric aging. *Atmos. Chem. Phys.* 18 (19):14017–14036. doi:10.5194/acp-18-14017-2018.

Shiraiwa, M., Li, Y., Tsimpidi, A.P., Karydis, V.A., Berkemeier, T., Pandis, S.N., Lelieveld, J., Koop, T., and Pöschl, U. (2017). Global distribution of particle phase state in atmospheric secondary organic aerosols. *Nat. Commun.* 8:15002. doi:10.1038/ncomms15002.

Wagner, F., Bortoli, D., Pereira, S., Costa, M.J., Silva, A.M., Weinzierl, B., Esselborn, M., Petzold, A., Rasp, K., Heinold, B., and Tegen, I. (2009). Properties of dust aerosol particles transported to Portugal from the Sahara desert. *Tellus, Ser. B Chem. Phys. Meteorol.* 61 (1):297–306. doi:10.1111/j.1600-0889.2008.00393.x.

Wang, B., Lambe, A.T., Massoli, P., Onasch, T.B., Davidovits, P., Worsnop, D.R., and Knopf, D.A. (2012). The deposition ice nucleation and immersion freezing potential of amorphous secondary organic aerosol: Pathways for ice and mixed-phase cloud formation. *J. Geophys. Res.* 117 (16):D16209. doi:10.1029/2012JD018063.

Zieger, P. and Va, O. (2017). Revising the hygroscopicity of inorganic sea salt particles. *Nat Commun* 8:15883. doi:10.1038/ncomms15883.